Low-temperature Crystal Structures and Magnetic Properties of the V_4-Cluster Compounds $Ga_{1-x}Ge_xV_4S_8$

Daniel Bichler, Herta Slavik, and Dirk Johrendt

Department Chemie und Biochemie, Ludwig-Maximilians-Universität München, Butenandtstraße 5 – 13 (Haus D), 81377 München, Germany

Reprint requests to D. Johrendt: E-mail: johrendt@lmu.de

Z. Naturforsch. **2009**, *64b,* 915 – 921; received May 27, 2009

Dedicated to Professor Ingo-Peter Lorenz on the occasion of his 65th birthday

Solid solutions $Ga_{1-x}Ge_xV_4S_8$ ($x = 0 - 1$) were synthesized by solid-state reactions and characterized by temperature-dependent X-ray powder diffraction and static magnetic susceptibility measurements. The compounds crystallize in the cubic $GaMo_4S_8$-type structure (space group $F\bar{4}3m$), built up by heterocubane-like $[V_4S_4]^{(5-x)+}$ cubes and $[Ga_{1-x}Ge_xS_4]^{(5-x)-}$ tetrahedra arranged in a NaCl-like manner. The successive substitution of Ga^{3+} by Ge^{4+} increases the electron count in the molecular orbitals (MO's) of the V_4-cluster gradually from seven to eight. We observe an almost linear increase of the magnetic moments, connected with a transition from ferromagnetic to antiferromagnetic ordering around $x \approx 0.5$. Remarkably, low-temperature structural phase transitions as known from the ternary compounds were also detected in the solid solutions. The gallium-rich compounds ($0 \leq x < 0.5$) undergo rhombohedral distortions like GaV_4S_8 (space group $R3m$), whereas distortions to orthorhombic symmetry (space group $Imm2$) as known from GeV_4S_8 occur in the germanium-rich part of the solid solutions ($0.5 \leq x \leq 1$).

Key words: Correlated Materials, Cluster, Spinel, Crystal Structure, Magnetism

Introduction

Transition metal chalcogenides with the cubic $GaMo_4S_8$-type structure [1, 2] have been a matter of increasing interest for years because of their physical properties, among them superconductivity under pressure [3, 4], metal-insulator transition [5], 4*d*-ferromagnetism [6], and various structural and magnetic instabilities at low temperatures [7 – 12]. All these phenomena reflect the strong coupling of structural, electronic and magnetic degrees of freedom in this system. Although the crystal structure of the compounds AM_4Q_8 (space group $F\bar{4}3m$; A = Ga, Ge; M = V, Ti, Nb, Ta; Q = S, Se) [13 – 17] can easily be derived from the spinel type AM_2Q_4 (space group $Fd\bar{3}m$) by an ordered half-occupation of the A site and a shift of the M site from 16*d* (5/8, 5/8, 5/8) to 16*e* (x, x, x), another description has turned out to be more useful [15]: As a consequence of the coordinate shift to $x \approx 0.6$, the transition metal atoms join to tetrahedral M_4 metal cluster units with strong metal-metal bonds. Thus the $GaMo_4S_8$-type structure of GaV_4S_8 can be described as a NaCl-like arrangement of $[V_4S_4]^{5+}$ cubes and $[GaS_4]^{5-}$ tetrahedra as depicted in Fig. 1.

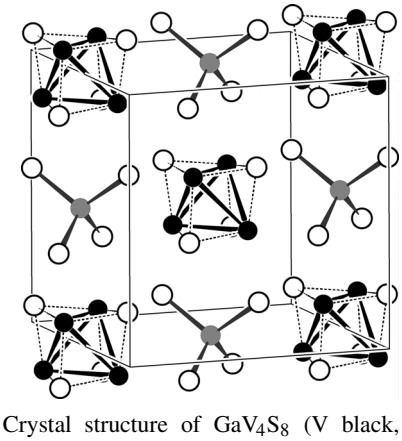

Fig. 1. Crystal structure of GaV_4S_8 (V black, Ga grey, S white).

The localization of electrons in metal-metal bonds causes non-metallic magnetic properties, and thus these materials represent a special class of Mott insulators [9]. In order to explain the magnetic insulating properties, we have introduced a concept of appropri-

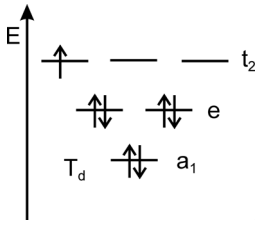

Fig. 2. Cluster MO scheme of cubic GaV_4S_8.

ate M_4 cluster molecular orbitals (MO's) [9, 15]. According to this, the metal centered electrons (*i. e.* those not involved in metal-ligand bonds) can occupy six bonding and six anti-bonding MO's. Thus the strongest *M–M* bonds are expected to occur when the bonding set is completely filled with 12 electrons. This is almost the case in $GaMo_4S_8$ with 11 electrons per Mo_4 according to an idealized ionic formula $Ga^{3+}(Mo^{3.25+})_4(S^{2-})_8$, whereas the cluster MO's of GaV_4S_8 are filled with seven electrons only as shown in Fig. 2. Since the three highest bonding MO's (t_2 set) are 3-fold degenerated with respect to the $\bar{4}3m$ symmetry of the cluster, one electron remains unpaired and induces the magnetic properties.

The MO cluster approach not only has allowed rationalizing the magnetism, but also explains the structural instabilities which appear frequently in this system. As an example, it has long been known that $GaMo_4S_8$ undergoes a structural distortion at 45 K [8], where the symmetry is reduced to $R3m$, and the Mo_4 cluster gets compressed along the 3-fold axis. On the other hand, the isotypic vanadium compound GaV_4S_8 also shows a rhombohedral distortion, but in this case the V_4-cluster becomes elongated [9]. The cluster-MO's allow to explain both effects by removing the degeneracy of the t_2 MO and stabilizing a particular structural distortion depending on the electron count.

Several studies have consistently shown that the structural and magnetic properties of $GaMo_4S_8$-type compounds are tunable by the variation of the cluster electron counts [18 – 20]. Among them, the different properties of GaV_4S_8 and GeV_4S_8 are remarkable. By adding only one electron to the V_4 cluster, the magnetic ordering changes from ferro- to antiferromagnetic, and the structural distortion of GeV_4S_8 leads to orthorhombic symmetry (space group *Imm*2) [11, 12] instead of rhombohedral as in GaV_4S_8 [9]. In this paper, we report the synthesis, crystal structures and magnetic properties of the solid solutions $Ga_{1-x}Ge_xV_4S_8$ in order to study the transition between these different behaviors in more detail.

Experimental Section

Synthesis

Powder samples of $Ga_{1-x}Ge_xV_4S_8$ were prepared by two-step syntheses. First, stoichiometric mixtures of gallium pieces (Alfa Aesar, 99.999 %), germanium pieces (Aldrich, 99.999 %) and vanadium powder (Smart Elements, 99.9 %) were heated at 800 °C (50 °C h^{-1}) in silica ampoules under argon atmosphere, until binary alloys $Ga_{1-x}Ge_xV_4$ were formed (1 – 3 heating runs). These precursors were then mixed with stoichiometric amounts of sulfur (Aldrich, 99.99 %), sealed in silica tubes under argon and heated to 750 °C (50 °C h^{-1}) for 12 h. The samples were then ground and heated subsequently until single-phase samples were obtained (1 – 3 heating runs).

Crystal structure determination

Powder patterns were recorded on a Huber G670 Guinier imaging plate diffractometer (Cu$K_{\alpha 1}$ radiation, Ge-111 monochromator) equipped with a closed-cycle He cryostat. Rietveld refinements were performed with the TOPAS package [21] using the fundamental parameters approach to the reflection profiles (convolution of appropriate source emission profiles with axial instrument contributions as well as crystallite microstructure effects). In order to describe small peak half width and shape anisotropy effects, the approach of Le Bail and Jouanneaux [22] was implemented into the TOPAS program, and the corresponding parameters were allowed to refine. The preferred orientation of the crystallites was described with spherical harmonics. An empirical 2θ-dependent absorption correction for the different absorption lengths of the GUINIER geometry was applied. As the background between 10 and 25° in 2θ shows artifacts from the low-temperature configuration of the GUINIER diffractometer, small sections of this range were excluded from the refinements.

Magnetic measurements

Magnetic properties of the samples were measured using a SQUID magnetometer (MPMS-XL5, Quantum Design Inc.). Finely ground powder samples were inserted into gelatine capsules of known diamagnetism and fixed in a straw as sample holder. The magnetic susceptibilities of the samples were collected in a temperature range from 1.8 to 300 K with magnetic flux densities up to 1 Tesla. Magnetization measurements with magnetic flux densities up to 5 T were recorded at different temperatures. The data were corrected for diamagnetic contributions of the capsule, the straw and the sample using diamagnetic increments [23] and analyzed using the Curie-Weiss law, modified by an additional temperature-independent contribution to the susceptibility χ_0:

$$\chi_{\mathrm{mol}} = \frac{C}{T-\theta_{\mathrm{cw}}} + \chi_0, \quad C = \mu_0 \frac{N_{\mathrm{A}}\mu_{\mathrm{B}}^2\mu_{\mathrm{eff}}^2}{3k_{\mathrm{B}}}$$

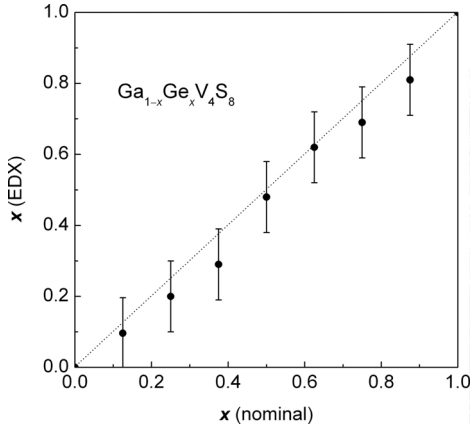

Fig. 3. Germanium contents of $Ga_{1-x}Ge_xV_4S_8$ obtained from EDX measurements *versus* the nominal compositions.

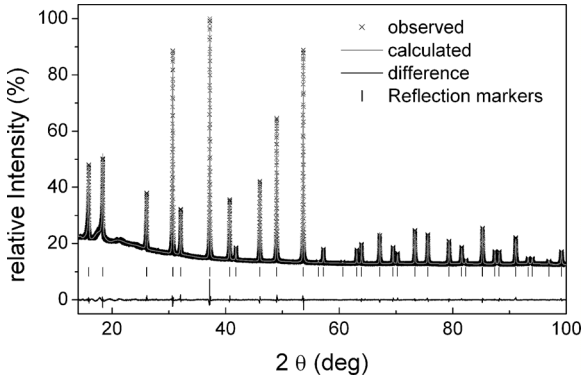

Fig. 4. X-Ray powder pattern and Rietveld fit of $Ga_{0.5}Ge_{0.5}V_4S_8$ measured at room temperature.

Results and Discussion

Crystal structures at room temperature

Room-temperature X-ray powder patterns of samples with the nominal compositions $Ga_{1-x}Ge_xV_4S_8$ (Δx = 0.125) could be completely indexed with cubic face-centered unit cells. The lattice parameters of GaV_4S_8 (966.1 pm) and GeV_4S_8 (965.5 pm) differ by only 0.6 pm. This is close to our experimental error, and therefore we were not able to deduce the composition reliably from the lattice parameters. However, a series of EDX measurements confirmed the nominal compositions within a tolerance of 10 %, as shown in Fig. 3. Rietveld refinements of all powder patterns were successful by using the structural parameters of GaV_4S_8 as an initial model; a typical fitted pattern is shown in Fig. 4. No indication of a deviation from full occupation of any site was detected. This was additionally confirmed by X-ray data of a single crystal with the nominal composition $Ga_{0.5}Ge_{0.5}V_4S_8$ not presented here. The results of the Rietveld refinements are compiled in Table 1.

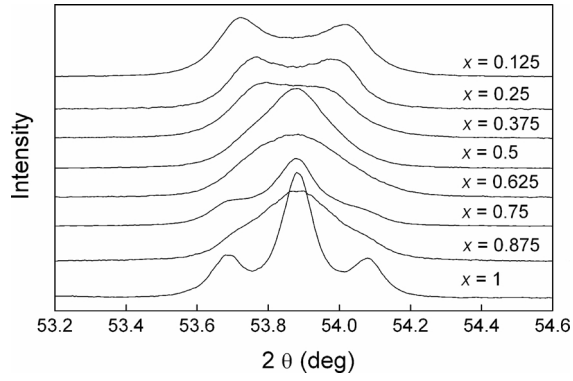

Fig. 5. Sections around the (440) reflections of $Ga_{1-x}Ge_xV_4S_8$ samples measured at 10 K.

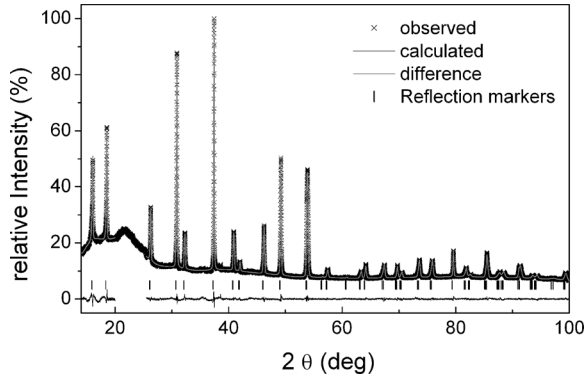

Fig. 6. X-Ray powder pattern and Rietveld fit of $Ga_{0.5}Ge_{0.5}V_4S_8$ measured at 10 K.

Crystal structures at low temperatures

Both ternary compounds GaV_4S_8 and GeV_4S_8 undergo second-order structural phase transitions at 38 and 30 K, respectively, in both cases well above the onset of magnetic ordering at 15 and 18 K. While GaV_4S_8 becomes rhombohedral (space group *R*3*m*), the low-temperature phase of GeV_4S_8 has orthorhombic symmetry (space group *Imm*2). A report by Chudo *et al.* about a rhombohedral (*R*3*m*) distortion of GeV_4S_8 was recently disproved [11]. In general, we have observed suppressions of the structural transitions in $GaMo_4S_8$-type compounds with mixed metal site occupations like $Ga_xV_{4-y}Cr_yS_8$ [18], $GaNb_{4-x}Mo_xS_8$ [19] and $GaV_{4-x}Mo_xS_8$ [24]. Since we do not introduce disor-

Table 1. Crystallographic data of $Ga_{0.5}Ge_{0.5}V_4S_8$ at 300 and 10 K.

Temperature	300 K	10 K	
Space group	$F\bar{4}3m$	$Imm2$	
Molar mass, g mol^{-1}	531.44	531.44	
Lattice parameters, pm	a = 965.24(3)	a = 683.66(2), b = 681.25(2), c = 964.54(1)	
Cell volume, nm^3	0.89923(8)	0.44923(2)	
Density, g cm^{-3}	3.925	3.929	
μ, mm^{-1}	54.2	54.2	
Z	4	2	
Data points	17201	16000	
Reflections	40	153	
d range, Å	1.005 – 6.320	1.005 – 6.320	
Excluded 2θ range(s), deg	–	20 – 25.5	
Constraints	1	6	
Atomic variables	7	16	
Profile variables	6	6	
Anisotropy variables	12	18	
Background variables	48	30	
Other variables	5	12	
R_P / wR_P	0.007 / 0.011	0.017 / 0.023	
R_{Bragg} / χ^2	0.006 / 1.634	0.005 / 1.134	
Atomic parameters:			
Ga/Ge	4a (0, 0, 0); U_{iso} = 82(1)	Ga/Ge	2b (0, 0, z); z = −0.0078; U_{iso} = 84(5)
V	16e (x, x, x)	V1	4c (x, 0, z)
	x = 0.60495(2); U_{iso} = 89(2)		x = 0.2181(7); z = 0.3845(4); U_{iso} = 89(3)
		V2	4d (0, y, z)
			y = 0.7944(3); z = 0.5936(5); U_{iso} = 89(3)
S1	16e (x, x, x)	S11	4c (x, 0, z)
	x = 0.36959(4); U_{iso} = 116(3)		x = 0.2600(9); z = 0.6163(5); U_{iso} = 101(3)
		S12	4d (0, y, z)
			y = 0.7443(5); z = 0.3539(5); U_{iso} = 101(3)
S2	16e (x, x, x)	S21	4c (x, 0, z)
	x = 0.86486(4); U_{iso} = 28(3)		x = 0.2753(8); z = 0.1189(5); U_{iso} = 101(3)
		S22	4d (0, y, z)
			y = 0.7289(5); z = 0.8536(6); U_{iso} = 101(3)
Selected bond lengths (pm):			
Ga/Ge – S2	225.9(1) × 4	Ga/Ge – S21	224.4(6) × 2
		Ga/Ge – S22	228.0(5) × 2
V – S1	229.8(1) × 3	V1 – S11	225.4(7)
		V1 – S12	231.2(5) × 2
		V2 – S11	227.3(5) × 2
		V2 – S12	233.7(7)
V – S2	254.2(1) × 3	V1 – S21	259.2(7)
		V1 – S22	249.7(5) × 2
		V2 – S21	253.8(4) × 2
		V2 – S22	254.8(7) × 2
V – V	286.5(1) × 3	V1 – V2	298.2(10)
		V1 – V1	287.3(5)
		V2 – V2	280.1(5)

der in the V_4-cluster units in the case $Ga_{1-x}Ge_xV_4S_8$, the structural distortions may rather persist.

In order to check for symmetry reduction, we have recorded X-ray powder patterns of all samples at 10 K. Broadening or even splitting of some reflections was observed, best visible for the (440) reflection close to 54°. We have shown earlier [11] that the splitting of this reflection in two components (220) and (208) indicates a rhombohedral distortion ($R3m$), whereas three components (400), (224), and (040) are only consistent with an orthorhombic lattice ($Imm2$). Fig. 5 shows the (440) reflections of the solid solutions in more detail. At low germanium contents (x = 0.125 – 0.375), we observe two peaks of identical intensity in agreement with the rhombohedral distortion as known from GaV_4S_8. The profile of $Ga_{0.5}Ge_{0.5}V_4S_8$ has already

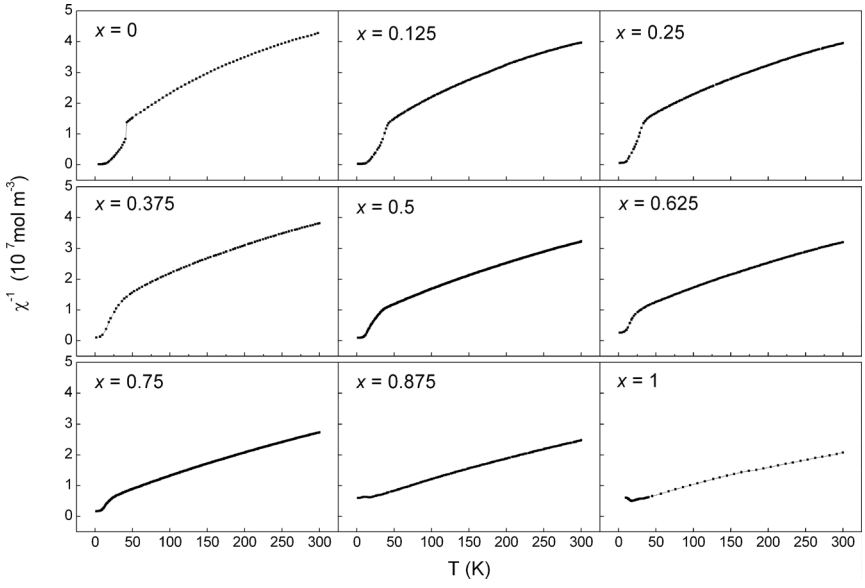

Fig. 7. Inverse magnetic susceptibility of $Ga_{1-x}Ge_xV_4S_8$ samples.

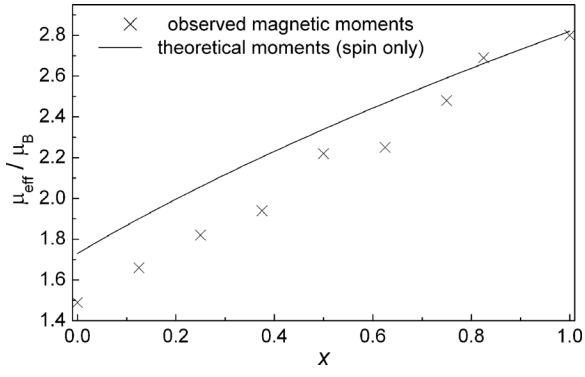

Fig. 8. Effective magnetic moments of $Ga_{1-x}Ge_xV_4S_8$.

Table 2. Magnetic data of $Ga_{1-x}Ge_xV_4S_8$.

x nominal	μ_{eff} (μ_B)	θ_{CW} (K)	χ_0 (mol^{-1} m^3)
0	1.52	−17	1.2×10^{-8}
0.125	1.66	−28	1.2×10^{-8}
0.250	1.82	−58	1.1×10^{-8}
0.375	1.94	−67	1.0×10^{-8}
0.500	2.22	−54	9.2×10^{-9}
0.625	2.25	−63	9.4×10^{-9}
0.750	2.48	−44	8.5×10^{-9}
0.875	2.69	−54	8.3×10^{-9}
1	2.80	−40	1.1×10^{-8}

three components (one central peak with two satellites), which are not yet separated due to the limited instrument resolution. With increasing germanium substitution, the three peaks become more separated, and the pattern is finally similar to that of the low-temperature phase of GeV_4S_8, which is included in Fig. 5 for comparison.

The low-temperature diffraction data unequivocally show structural distortions in all samples of the series $Ga_{1-x}Ge_xV_4S_8$. We observe a gradual transition from rhombohedral distortions known for GaV_4S_8 to orthorhombic lattices as observed in GeV_4S_8 with an inflection close to $Ga_{0.5}Ge_{0.5}V_4S_8$. Fig. 6 shows the Rietveld fit of $Ga_{0.5}Ge_{0.5}V_4S_8$ at 10 K. The structural data of the low-temperature phase GeV_4S_8 (space group *Imm*2) [11] have been used as initial parameters, and the refinements resulted in very similar structural parameters for $Ga_{0.5}Ge_{0.5}V_4S_8$. As for the pure germanium compound, the distortion is mainly caused by the change of the ideal V_4 tetrahedron into a butterfly-like structure, where one V–V edge is shortened by 6.5 pm, and the opposite edge is elongated by 2.5 pm. This clearly demonstrates the identical distortion motifs of $Ga_{0.5}Ge_{0.5}V_4S_8$ and GeV_4S_8, and we can safely assume the same also for samples with higher germanium contents ($x > 0.5$).

Magnetism

The inverse magnetic susceptibilities of the $Ga_{1-x}Ge_xV_4S_8$ samples are displayed in Fig. 7. The decreasing slopes of the curves above 100 K indicate the gradual filling of the V_4 cluster orbitals that yield increased magnetic moments. We find an almost linear dependency of the effective magnetic moments μ_{eff} on the germanium content as shown in Fig. 8, in agree-

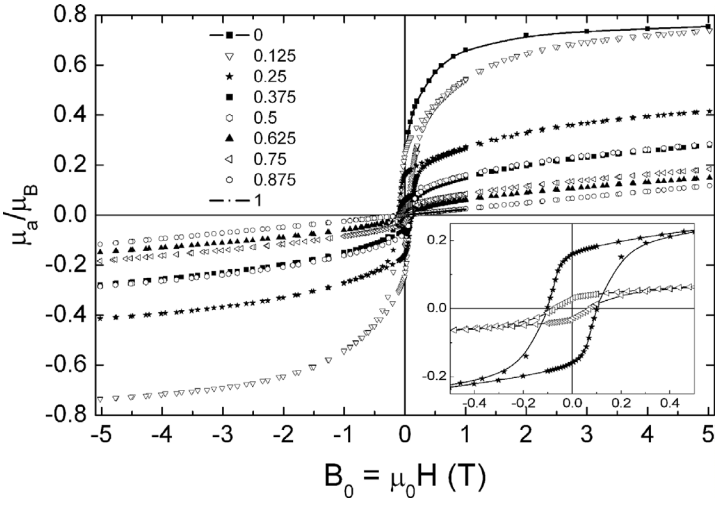

Fig. 9. Isothermal magnetization of $Ga_{1-x}Ge_xV_4S_8$ samples.

ment with expectations from the cluster MO approach. The magnetic data extracted from the Curie-Weiss analysis are collected in Table 2. Anomalies in the χ^{-1} *vs.* T plots appear around 30 K in all cases, but more pronounced in gallium-rich samples. These more or less sharp drops are caused by the second-order structural phase transitions. In the course of these transitions, the V_4 cluster MO's become reorganized according to the lowered symmetry, *i. e.* space group *R*3*m* for $x < 0.5$ and space group *Imm*2 for $x \geq 0.5$, as shown in the previous chapter.

Fig. 9 shows the isothermal magnetization curves measured at 1.8 K. We observe a gradual transition from ferromagnetic to antiferromagnetic behavior as the germanium fraction increases. The magnetization of the samples with compositions $0.25 \leq x \leq 0.75$ (insert in Fig. 9) still shows typical ferromagnetic saturation and hysteresis, but the moments decrease strongly with x. Since we can assume certain (small) inhomogeneities in the Ga/Ge distributions, we suggest that the observed curves are superpositions of Ge-rich antiferromagnetic and Ga-rich ferromagnetic domains, which accumulate to the observed magnetic moments. The magnetization of $Ga_{0.25}Ge_{0.75}V_4S_8$ is reminiscent of the behavior of an antiferromagnetic phase with small ferromagnetic contamination, while the curve for $Ga_{0.125}Ge_{0.875}V_4S_8$ finally is almost linear as expected for an antiferromagnet.

Acknowledgement

This work was financially supported by the Deutsche Forschungsgemeinschaft.

[1] H. Barz, *Mater. Res. Bull.* **1973**, *8*, 983.
[2] C. Perrin, R. Chevrel, M. Sergent, *C. R. Acad. Sci., Ser. C. Chim.* **1975**, *280*, 949.
[3] R. Pocha, D. Johrendt, B. Ni, M. M. Abd-Elmeguid, *J. Am. Chem. Soc.* **2005**, *127*, 8732.
[4] M. M. Abd-Elmeguid, B. Ni, D. I. Khomskii, R. Pocha, D. Johrendt, X. Wang, K. Syassen, *Phys. Rev. Lett.* **2004**, *93*, 126403/1.
[5] C. Vaju, L. Cario, B. Corraze, E. Janod, V. Dubost, T. Cren, D. Roditchev, D. Braithwaite, O. Chauvet, *Adv. Mater.* **2008**, *20*, 2760.
[6] A. K. Rastogi, A. Berton, J. Chaussy, R. Tournier, M. Potel, R. Chevrel, M. Sergent, *J. Low Temp. Phys.* **1983**, *52*, 539.
[7] O. Pena, H. Ben Yaich, M. Potel, M. Sergent, *Physica B: Cond. Matter* **1990**, *163*, 435.
[8] M. Francois, W. Lengauer, K. Yvon, H. Ben Yaich-Aerrache, P. Gougeon, M. Potel, M. Sergent, *Z. Kristallogr.* **1991**, *196*, 111.
[9] R. Pocha, D. Johrendt, R. Pöttgen, *Chem. Mater.* **2000**, *12*, 2882.
[10] S. Jakob, H. Müller, D. Johrendt, S. Altmannshofer, W. Scherer, S. Rayaprol, R. Pöttgen, *J. Mater. Chem.* **2007**, *17*, 3833.
[11] D. Bichler, V. Zinth, D. Johrendt, O. Heyer, M. K. Forthaus, T. Lorenz, M. M. Abd-Elmeguid, *Phys. Rev. B* **2008**, *77*, 212102.
[12] H. Müller, W. Kockelmann, D. Johrendt, *Chem. Mater.* **2006**, *18*, 2174.
[13] D. Brasen, J. M. Vandenberg, M. Robbins, R. H. Willens, W. A. Reed, R. C. Sherwood, X. J. Pinder, *J. Solid-State Chem.* **1975**, *13*, 298.

[14] H. Haeuseler, S. Reil, E. Elitok, *Int. J. Inorg. Mat.* **2001**, *3*, 409.
[15] D. Johrendt, *Z. Anorg. Allg. Chem.* **1998**, *624*, 952.
[16] C. Vaju, J. Martial, E. Janod, B. Corraze, V. Fernandez, L. Cario, *Chem. Mater.* **2008**, *20*, 2382.
[17] H. Ben Yaich, J. C. Jegaden, M. Potel, M. Sergent, A. K. Rastogi, R. Tournier, *J. Less-Comm. Met.* **1984**, *102*, 9.
[18] D. Bichler, D. Johrendt, *Chem. Mater.* **2007**, *19*, 4316.
[19] S. Jakob, Dissertation, Ludwig-Maximilians-Universität, München, **2007**.
[20] H. Ben Yaich, J. C. Jegaden, M. Potel, M. Sergent, A. K. Rastogi, R. Tournier, *J. Less-Comm. Met.* **1984**, *102*, 9.
[21] A. Coelho, TOPAS-Academic (version 4.1), Coelho Software, Brisbane, **2007**.
[22] A. Le Bail, A. Jouanneaux, *J. Appl. Crystallogr.* **1997**, *30*, 265.
[23] H. Lueken, *Magnetochemie*, Teubner, Stuttgart, Leipzig, **1999**.
[24] A. V. Powell, A. McDowall, I. Szkoda, K. S. Knight, B. J. Kennedy, T. Vogt, *Chem. Mater.* **2007**, *19*, 5035.